Available online at www.sciencedirect.com
SCIENCE DIRECT®
Journal of Nuclear Materials 323 (2003) 220–228
journal of nuclear materials
www.elsevier.com/locate/jnucmat

Stability and mobility of defect clusters in copper under displacement cascade conditions

Hiroaki Abe [a,b,*], Naoto Sekimura [b], Yunmin Yang [b]

[a] Research Center for Nuclear Science and Technology (RCNST), University of Tokyo, Shirakata Shirane 2-22, Tokai, Naka, Ibaraki 319-1188, Japan

[b] Department of Quantum Engineering and Systems Science, University of Tokyo, Hongo 7-3-1, Bunkyo, Tokyo 113-8656, Japan

Abstract

The recent molecular dynamics (MD) simulations have provided insights into the nature of displacement cascades, revealing defect cluster formation and their stability. In order to get direct experimental insights into the defect accumulation processes, in situ TEM observations in copper under irradiations with 100 keV C^+ and 240 keV Cu^+ ions at temperatures from 573 to 823 K were performed. Defect clusters produced by cascades were observed to be unstable with lifetimes of seconds, which depend on temperature, ion species and fluence. Multiple (2 or 3) defect clusters showing up their contrast in the same video frames, having a time resolution of 1/30 s, were concluded to be features related to subcascades and fast diffusion of defect clusters when located within 30 nm and from 30 to 140 nm, respectively. The detailed analysis of the defect cluster distribution shows that the direction of the fast diffusion is strongly related to crowdion directions, suggesting that the mechanism is based on motion of crowdion bundles. Instability and diffusion of defect clusters detected under ion irradiation are interpreted in terms of transformation into crowdion bundles, which is well described by MD simulations of dislocation loop stability under a compressive stress.

PACS: 61.72.Ff; 61.80.Jh

1. Introduction

Energetic particles, like ions and neutrons, transfer their energy to lattice atoms as kinetic energy or as electronic excitation, and result in lattice displacements. When kinetic energy of more than a few keV is transferred to a primary knock-on atom, a bunch of displacements is generated, forming the so-called displacement cascade. Extremely high energy density is introduced in the cascade volume, resulting in formation of secondary defects, such as defect clusters or amorphous zones. Since the secondary defects are observable in transmission electron microscopy (TEM) as strain or phase contrast features, accumulation process and instability of such clusters under ion irradiations have been investigated in copper [1–3], nickel [3,4], gold [3,5,6] and semiconductors [7] using transmission electron microscopes interfaced with ion accelerators [8–10]. The fraction of surviving clusters, as well as their size, depends on irradiation conditions, such as incoming particles, substrates and temperature [4,11]. Defect clusters are also formed by electron irradiations when the energy of electrons is high enough. The clustering process is based on accumulation of point defects, which can induce cluster nucleation and growth processes. Recent observations successfully detected motion of defect clusters in metals under 1 MeV electron irradiations [12,13]. The motion suggests that dislocation loops transform into mobile clusters enabling diffusion with relatively low activation energy. However, its mechanism has not been clarified yet experimentally. Recent molecular dynamics (MD) simulations have revealed the generation of crowdion bundles at the periphery of

* Corresponding author. Address: Research Center for Nuclear Science and Technology (RCNST), University of Tokyo, Shirakata Shirane 2-22, Tokai, Naka, Ibaraki 319-1188, Japan.
E-mail address: abe@utnl.jp (H. Abe).

0022-3115/$ - see front matter © 2003 Elsevier B.V. All rights reserved.
doi:10.1016/j.jnucmat.2003.08.006

cascades in metals [14]. Especially in copper it is reported that only interstitial-type dislocation loops transform into crowdion bundles, while both interstitial- and vacancy-type ones do so in iron [15]. The crowdion bundles are capable of traveling large distances along the crowdion directions, i.e. $\langle 1\,1\,0\rangle$ in fcc and $\langle 1\,1\,1\rangle$ in bcc. The activation energy of the crowdion-bundle motion is extremely small, below 0.04 eV, which is smaller than the binding energy of the clusters and than the migration energy of single interstitials. Therefore, once the crowdion bundles are formed, their migration could be observed even at low temperatures [12,16]. But their formation directly from a displacement cascade is obviously impossible to be observed by the conventional post-irradiation TEM work. Our recent in situ TEM work [17,18] was successful to simultaneously observe cascade-driven defect clusters in metal substrates (Cu and Au) implanted with carbon ions at 570–970 K, and to synthesize spherical graphitic clusters, so-called carbon onions [19]. Even though the implantations were performed in thin TEM foils at high temperatures and implanted carbon is an immiscible element in the metals, the carbon clusters were formed inside of the TEM foils, not at surface [19]. The results indicate that impurity-defect interactions affect the damage evolution process, as previously observed in the case of irradiation-induced segregation in intermetallic compounds [20]. The objectives of this work are, therefore, by in situ TEM observations in Cu under irradiation with C^+ and Cu^+ ions, to study the formation and the stability of defect clusters, to get experimental evidence on the formation and fast diffusion of the crowdion bundles, and to get insights into the impurity effects on the formation and the stability of cascade-driven defect clusters.

2. Experimental procedures

Pure copper (>99.999%) annealed at 1000 K for 12 h in Ar–3%H_2 gas flow was cut into disks of 3 mm in diameter. The specimens were then electrochemically perforated to achieve electron transparent thin foils in a solution of 30% nitric acid in methanol at 20 V and 277 K. Prior to irradiation, samples were set in TEM and annealed at 773 K or above in order to stabilize surface morphology under irradiation at high temperatures. Because copper has a rather high vapor pressure in vacuum and the ion irradiation enhances evaporation, surface morphology of sample changed significantly above 770 K, especially under high beam current. Samples whose surface normal is close to $\{0\,0\,1\}$ were relatively stable during annealing and irradiation in the TEM, while $\{0\,1\,1\}$ and $\{1\,1\,1\}$ surfaces did not suit this work because of their significant evaporation. They were then irradiated with ions in a TEM (JEM-4000FX, JEOL Ltd.) conducted with an ion accelerator at Takasaki Ion Accelerators for Radiation Application (TIARA) at Japan Atomic Energy Research Institute (JAERI) – Takasaki [10,21]. Irradiation was performed with 100 keV C^+ ions and a current of 2.5×10^{13} C/cm^{2}s, or 240 keV Cu^+ ions and 5.1×10^{11} Cu/cm^{2}s at temperatures ranging from 573 to 823 K. Taking into account the irradiation geometry, in which the angle between the ion beam and the sample normal is 30°, projected ranges from the sample surface were estimated by TRIM [22] calculations as 115 and 57 nm for carbon and copper ions, respectively. Since the thickness of the observed regions was typically 50–70 nm, roughly 81–89% and 31–58% of incoming carbon and copper ions penetrate the sample, respectively. Microstructural evolution was observed mainly with the weak-beam dark-field technique ($n = [0\,0\,1]$, $g = 200$, $g(4\text{–}6g)$). The imaging system (Gatan Inc., model 676) consists of a YAG scintillator screen fiber-optically coupled to an image intensifier and then further to a conventional TV-rate CCD (frame rate of 1/30 s). The image was videotaped without image processors so as to achieve the maximal time resolution. Effect of remanence of the scintillator is not experimentally detected in the system. Contrast and brightness of each frame were the only parameters that were modified in a computer after image acquisition.

To reveal the stability of defect clusters, we have performed MD simulations on various sizes of dislocation loops in copper lattice under compressive stress. A copper lattice of $30\times30\times33$ in units of lattice constant (120 000 atoms) was set up and the long-range Finnis–Sinclair EAM potential was used. The compression was performed at 0 K along $[\overline{0.09}\ 0.42\ 0.91]$ by the displacement-controlled manner. This setup minimizes the thermal fluctuation and makes the $(1\,1\,1)$ plane and $[1\,0\,\bar{1}]$ direction the most favorable slipping system. For each load step, the incremental strain of 0.3% was applied along the axis 2 by 1 time step (5 fs) and relaxed for 5000 time steps. Dislocation loops, consisting of self-interstitial atoms (7–187 atoms) on $(1\,1\,1)$ habit planes with a Burgers vector of $1/3\langle 1\,1\,1\rangle$ were put at the center of the crystal. To visualize the lattice defect we employed an energy screening method to analyze the overall evolution process of loops, dots in the following figure represent atoms with potential energies higher than −3.47 eV whereas the perfect lattice atoms have a potential energy of −3.498 eV.

3. Results and discussion

3.1. Microstructural evolutions

Microstructural evolution during ion irradiations is described in the following. Firstly, defect contrast features appeared, as shown with black arrows in Fig. 1. Defects were observed as dot or black-and-white

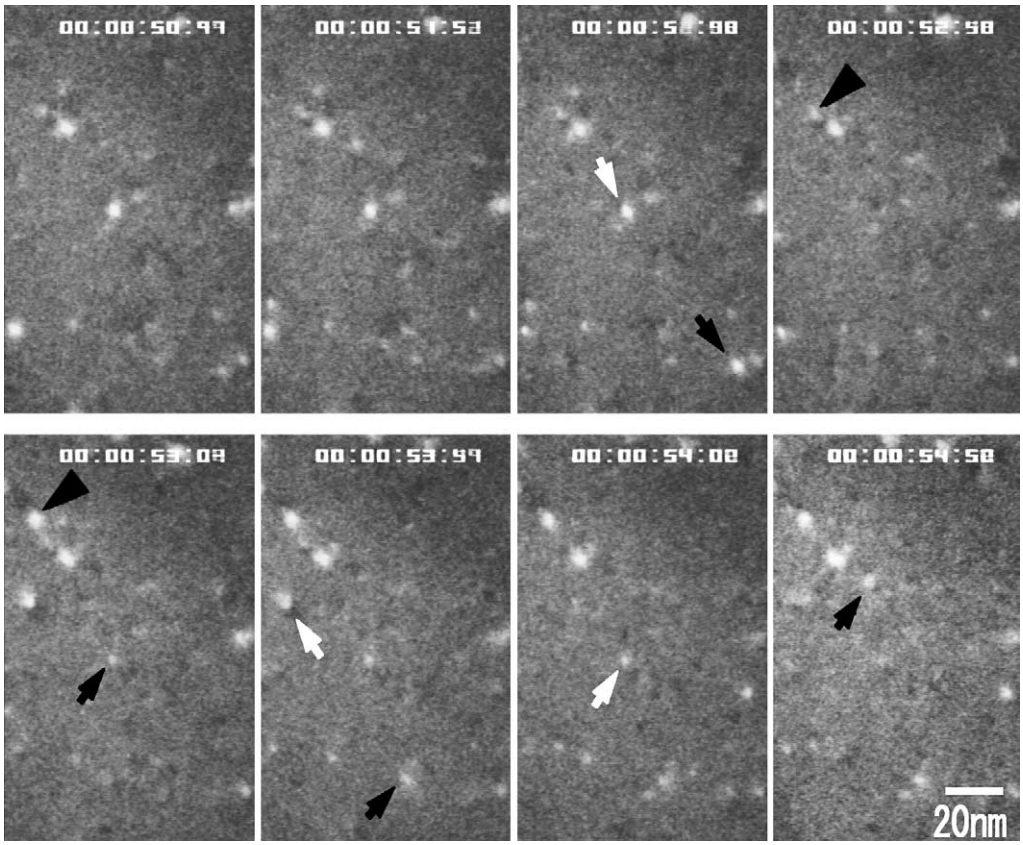

Fig. 1. Microstructural evolution in copper irradiated with 100 keV C^+ ions at 573 K. Ion beam current one the sample is 2.0 nA/0.25 mmϕ (2.5×10^{13} ions/cm^{2}s). The sequence is captured from videotapes whose time resolution is 1/30 s. The black and white arrows show formation and annihilation of defect clusters, respectively, while the black large arrow show motion of defect clusters.

contrast features, whose size ranged from 4 to 6 nm in diameter. The nature of defects is presumed to be vacancy-type dislocation loops, SFT and interstitial-type dislocation loops. Probability of defect cluster formation was estimated to be 2% and 67% of incoming particles for carbon and copper ion irradiations, respectively. The result is reasonable considering defect density in an individual cascades [23], which is 0.14 and 2.1 vacancies/nm^3, respectively, as calculated by TRIM.

We can suppose that high energy cascades result in defect clusters visible in TEM. Taking into account the sample thickness, formation rate of defect clusters is 0.1 and more than unity per ion of C and Cu irradiation, respectively. This result indicates, especially in Cu irradiation, that an ion produces defect clusters resulting from subcascade or from other mechanisms. Indeed, in addition to the single contrast features, multiple (typically 2 or 3) contrast features appeared in video frames, each of which is located at distances from 4 to 140 nm as shown in Fig. 2(a) and (b). Fig. 3(a) and (b) show distributions of distance between defect clusters appearing in the same video frame, and yield of angles, respectively. The angle is defined counterclockwise between the segment between the two clusters and the horizontal direction in the video frame. It is seen that distance distributions range up to 140 nm, and that angle distributions especially in the features of more than 20 nm are anisotropic. Such a multi-defect formation is either due to fast diffusion of defect clusters or subcascade formation, both of which will be clarified later.

Secondly, a specific feature to be mentioned is the instability of defect clusters under ion irradiation as shown in Fig. 4. Stable defects were first formed and eventually transformed into mobile defects. Some migrated one-dimensionally back-and-forth with an amplitude of about 5 nm and a frequency of 1 s^{-1} or more, and the others were in motion in one direction with velocities ranging from 50 to $>10^3$ nm/s. At the onset of motion, some of the defects loose their strong strain contrast. Such contrast transition may be the result of transition to a mobile defect cluster, which presumably has less strain field in the surrounding volume, although authors must mention similar phenomenon can be observed due to a persistence of vision in a frame (1/30 s) if

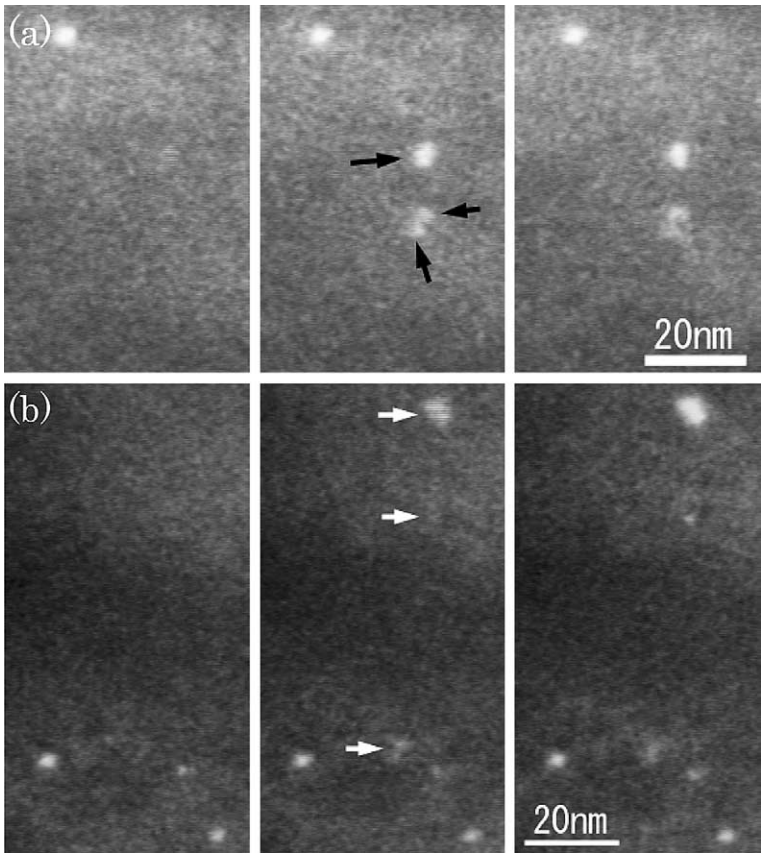

Fig. 2. Microstructural evolution in copper irradiated at 828 K with 240 keV Cu^+ ion flux of 5.1×10^{11} ions/cm^{2}s. Two defect clusters appeared relatively closer (typically <30 nm) in the same video frame in (a). Three defect clusters appeared relatively further (typically from 30 to 140 nm) in (b). See text for detail discussion.

a high-contrast object has moved fast enough. Some of the defect clusters migrate in a single way. The rate ranged roughly from 70 to $>10^3$ nm/s. For both moving behaviors their directions appeared to be anisotropic. Similar phenomena have been reported in iron under 1 MeV electron irradiation [12,13].

Thirdly, defects eventually disappeared in seconds. Their lifetime depended on incident particles, temperature and irradiation fluence. Fig. 5 shows defect lifetime in copper irradiated with (a) Cu ions and (b) C ions at 673 K. Differences in defect lifetime under C irradiations appeared with irradiation time. The averaged lifetime was 1.2 s at the early stage of implantation (7 min or 1.2×10^{16} ions/cm^2). After more than 12 min (2.0×10^{16} ions/cm^2), the lifetime became 4.4 s. In case of self-ion irradiation, the averaged lifetime was 5.5 s and the distribution was nearly identical during irradiation time up to 11 min. For the observation of the above multi-defect formation, the irradiation temperatures from 670 to 820 K were identical because of the reasonable lifetime and morphological stability under irradiation. Through the detail observations it is found that the defect lifetime depends on the nature of defect clusters. Typical lifetime of SFT is several seconds and more. Note that, in addition to SFT, we observed two kinds of lifetime behavior in 240 keV Cu^+ irradiation in Fig. 5. The one has the lifetime from 2 to 10 s and the other has less than 1 s. The majority of the latter one is less than several thirtieths. The nature-dependent lifetime has been reported by Ishino et al. [5] in gold in the beam-off condition. They claimed that vacancy-type loops and SFT were observed by bright-field technique. We observed the same behavior in gold irradiated with copper ions. The WBDF observation revealed that there are three kinds of defect clusters, one of which was missed in the beam-off condition because of the very short lifetime (several thirtieths). The detail will be reported elsewhere. The difference in the lifetime and taking into account the temperature of irradiation (stage IV–V), we conclude that the nature of the short-lifetime features is presumably of interstitial type.

Fourthly, accumulation of implanted species affects defect-cluster lifetime as well as cluster formation rate, besides point defects were found to be less effective.

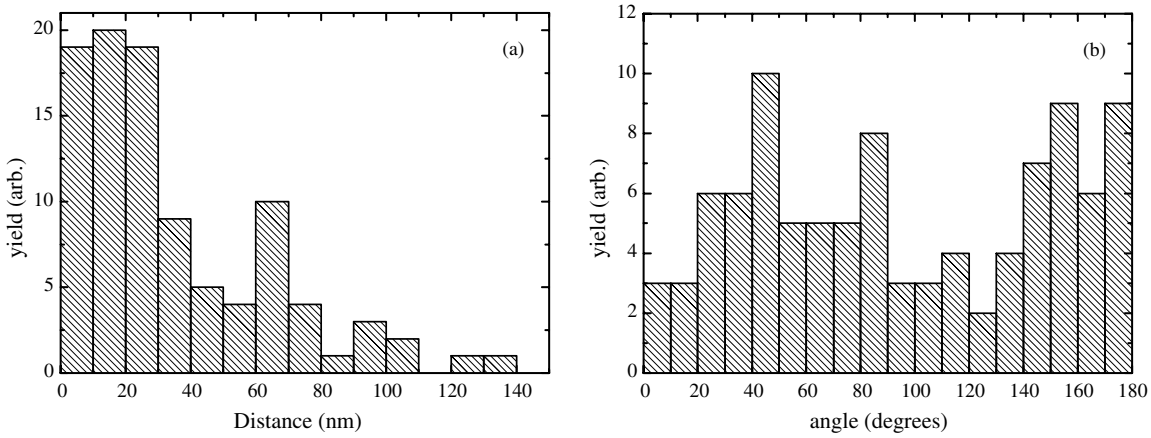

Fig. 3. Distribution of the multiple-defect clusters appeared in the same time bins (the same video frames) as a function of distance and angle in (a) and (b), respectively, in copper irradiated with 240 keV Cu^+ ion flux of 5.1×10^{11} ions/cm^{2}s at 828 K. Two peaks at 20 and 70 nm are evident in (a). Anisotropic distribution is seen in (b) and each peak corresponds to a projected $\langle 1\,1\,0\rangle$ direction.

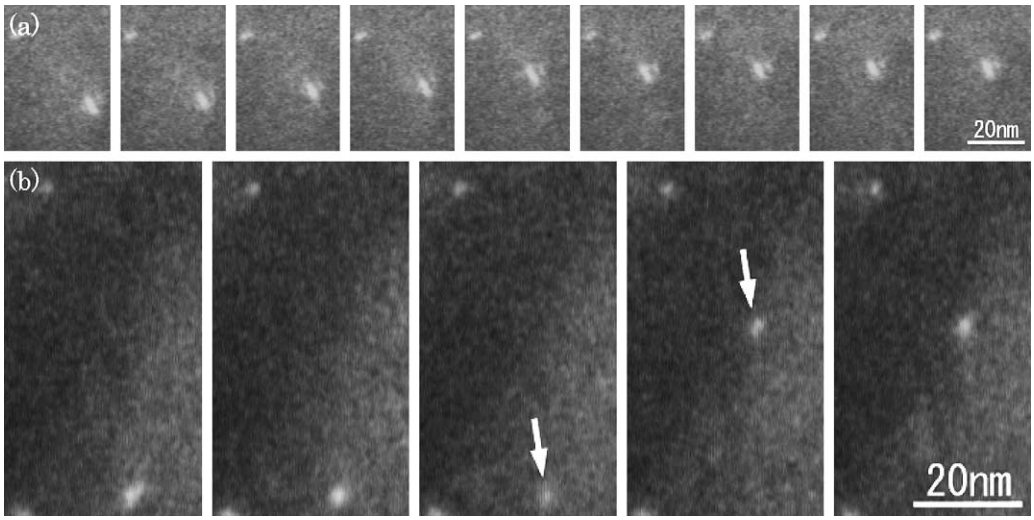

Fig. 4. Microstructural evolution in copper irradiated with 240 keV Cu^+ ion flux of 5.6×10^{11} ions/cm^{2}s at 878 K and of 5.1×10^{11} ions/cm^2 s at 828 K in (a) and (b), respectively, showing relatively slow diffusion of a defect cluster with stacking-fault-like contrast, and fast diffusion (>10^3 nm/s) of a defect cluster.

Since carbon is an insoluble element in copper, the majority of implanted carbon ions diffuse towards top and bottom surfaces of TEM thin foils. As shown in Fig. 5, implanted species presumably behaved so in the first minutes, resulting in short lifetime of defect clusters under carbon implantation. The implanted ions altered the cluster lifetime as well as the formation rate. At the fluence of the order of 10^{16} C/cm^2, the lifetime extends to tens of seconds, while the formation rate decreased by 20% from that at the beginning of irradiation. At the high fluence, defect complexes of carbon with point defects gradually accumulated in samples, attributable for the lower diffusion rate of point defects and for the longer lifetime of defect clusters. Indirect but good evidence for the model is the nucleation of graphitic clusters under the same conditions [24]. Roughly 5-nm spherical clusters consisting of 7×10^3 carbon atoms were formed *inside* the TEM thin foil at the implantation time of 20–40 min, although the nucleation time is strongly affected by sample geometry.

3.2. Subcascade formation

One characteristic feature in high-energy and heavy ion irradiation is the branching off of the displacement sequences forming multiple displacement-condensed

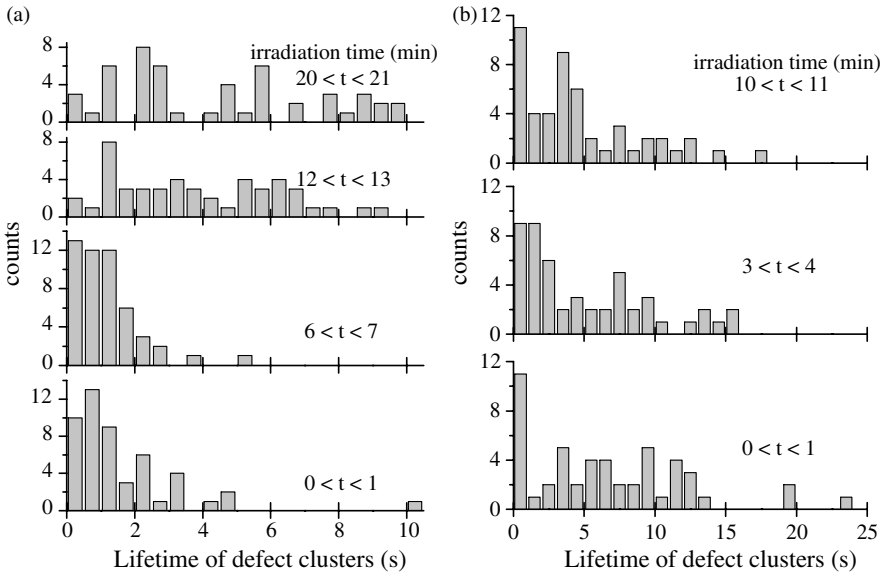

Fig. 5. Lifetime of defect clusters as a function of irradiation time in copper irradiated with 100 keV C^+ and 240 keV Cu^+ ions in (a) and (b), respectively, at 828 K.

regions along a trajectory of an ion, so called subcascades. The WBDF method employed in this work is a helpful to observe subcascades since it enhances contrast around defects resulting in higher resolution in distinguishing closely located contrast features [25]. Fig. 2(a) shows a sequence of 240 keV Cu^+ ion irradiation with a time difference of 1/30 s. Three tiny clusters appeared at the same time, and they were typically located within 30 nm or less as shown in Fig. 3. The phenomena were characteristic to Cu-ion irradiations, while under the C-ion irradiation they have never been detected. To clarify the observed phenomena, the probability that multiple independent ions pass through and form defect clusters within such tiny areas is estimated. Since the ion flux is 5.1×10^{-3} Cu/nm^{2}s, the probability that an ion hits the area of 20 nm in diameter in a time bin of 1/30 s is 0.035, when a defect formation rate of 0.67 is taken into account. Therefore, the frequency at which two or three ions hit the small regions in the same time bin is 1.2×10^{-3} or 4.3×10^{-5}, respectively. On the other hand, in case of carbon ion irradiation, it is estimated as 2.8×10^{-3} or 1.5×10^{-4}, respectively, which is much higher than those of copper. However, fewer events have been detected in C^+-irradiations than Cu^+ ones. Hence, we conclude the multiple contrast features appeared at the same video frame are the result of single ion events, i.e. subcascade formation and their clustering, as will be seen in the following.

For further evaluation of subcascades, Monte-Carlo simulation (TRIM) was performed to compare individual and transport cascades. The logic of calculation is based on Ref. [23], taking into account individual displacement events. Averaging over 50 individual cascades and defining cascade volume as three-dimensional standard deviations of collision coordinates, the major and minor axes of individual cascades are 22 and 7 nm in Cu irradiated with 240 keV Cu, respectively. On the other hand, those in Cu irradiated with 100 keV C are 43 and 11 nm, respectively. Volume fraction of individual cascades are of the order of 10^{-4} and 10^{-2} for the transport cascades of Cu and C ions, respectively, both indicating that displacements are rather condensed along the trajectories of incoming ions. Supposing 10 or 20 keV as the threshold energy of subcascade formation, the averaged distance of subcascades was estimated as 20 and 23 nm, respectively, in Cu-ion irradiations. Fairly good agreement between the TRIM calculations and the experimental results indicates the multiple clustering features are the result of subcascade formation. In the experiments we detected roughly one subcascade per second in videotaped image; i.e. 0.008 subcascades/ion, on the other hand, about 0.3 subcascade/ion in TRIM calculation. Such large difference is thought to be attributed to sample temperature and high concentration of point defects in matrix, which enhance the recombination of interstitials and vacancies. The detailed analysis with TRIM, such as energy density of individual subcascades, will give further insights into the threshold energy of the *effective* subcascade formation rate.

3.3. Formation of fast-moving defects

Recent molecular dynamics (MD) simulations [14] predicted the formation of crowdion bundles at the

periphery of cascades. However, no experimental evidence has been available, because of their extremely low activation energies. The in situ TEM observation is one of the possible experiments to get insights into the cascade-driven defect clusters. In Fig. 3(a), in addition to the subcascade-driven defect clusters being located in small groups of less than 30 nm in size, a number of defect clusters located far away was also detected. The frequency of two-particle event in a region of, for example, 100 nm is 0.80. But the possibility of multi-particle event can be eliminated in the following reasons. The one is that, as shown in Fig. 3(b), anisotropic distribution of multi-defect events is evident. The three peaks in the figure are almost identical to projections of $\langle 1\,1\,0\rangle$ crowdion directions. Supposing a multi-particle event, the distribution should be isotropic because of its randomness. The other reason is that distance between such defects varies with irradiation time. At the beginning of irradiation, the distance ranges to 140 nm, and it decreases with increasing irradiation time. Difference in the formation rate is also seen in the figure. From those reasons, we conclude that the evolution of multi-defect formation in the same time bin results from single particle event. The nature of the defects has not yet been identified in this work. Majority of defect clusters observed in our experiments are thought to be vacancy type clusters, which have been observed by Ishino et al. [3]. However, the defects being discussed in this section are presumably interstitial-type because of the following reasons: They are rather smaller and less stable (lifetime $<$ several thirtieth) than the vacancy-type clusters as discussed previously, therefore impossible to observe in bright-field technique. The time-dependent formation rate was quite different from that of vacancy-type. They were observed in the area with thickness of 50–100 nm, and none in the thin area. This behavior suggests that the defects are of interstitial type; though the last one can be both from point defect concentration and geometry. Since there seems to be no valid mechanism to describe such long-range phenomena, and since the irradiation-time dependence indicates that they are diffusion-controlled, crowdion bundles formed at the cascade are presumably attributable to the phenomena. Further, we must mention that this is so a long range defect evolution mechanism firstly observed, and must be taken into account in the microstructure evolutions under irradiations with neutrons and ions.

Because of the low activation energy for the crowdion bundle diffusion [15], extremely large diffusion length can be expected, such as microns in 1/30 s, even at low temperature. Note that this estimation is invalid in the materials kept at high temperature and even under irradiations, where high concentration of point defects, small defect clusters, impurities and even the fluctuation of atomic arrangement work as diffusion obstacles. As mentioned previously, and as clearly recognized in Fig. 5, diffusion distance depends on irradiation time and implantation fluence, which directly relate to the lattice defect concentration. Although theoretical explanations on the time-dependent diffusion distance are unavailable, we expect that application of point defect kinetics under electron irradiations [26] and under displacement cascade conditions [27], as well as MD simulations, may reveal the nature of the obstacles.

3.4. Transformation of sessile loops into crowdion bundles in MD

Dislocation loops, consisting of self-interstitial atoms (7–187 atoms) on (1 1 1) habit planes with a Burgers vector of $1/3\langle 1\,1\,1\rangle$ were put at the center of the crystal, and stress applied to reveal their stability. The detail of the study will be reported elsewhere [28]. Since the incremental strain rate is so high, which is equivalent to the order of 10^8/s in deformation rate, the microstructural behavior can be qualitatively represented, but the value of stress is much higher than the experimentally observed ones. Sessile loops were unstable at the yield stress, and transformed into crowdion bundles. Fig. 6 shows the behavior of a dislocation loop consisting of 19 atoms under plastic deformation. This transformation leads to the yield drop in the stress–strain curve. The formation of a crowdion bundle at yield stress and its diffusion and propagation along $[1\,0\,\bar{1}]$ are clearly observed in Fig. 6(d) and (e). Two sets of crowdion bundles were formed and diffuse in the opposite directions in (1 1 1) planes so as to release the applied stress. The behavior does not depend on loop size up to 3.4 nm (64 atoms). In the case of a 19-atom loop, the potential difference between a dislocation loop and a crowdion bundle is estimated as 0.03 eV/atom, which is equivalent to 1% of plastic deformation in the lattice. It should be noted that insignificant potential barriers has been detected through the transformation.

The experimental results in the previous sections, Fig. 4 in particular, can be interpreted as (1) dislocation loops transform into mobile defect clusters, (2) diffuse along $\langle 1\,1\,0\rangle$ directions, and (3) transform into loops again. The MD results in this work clearly simulate (1) and partly (2) in this process. The results indicate a sessile loop transform into crowdion bundles at relatively low stress without potential barrier. The direct MD simulation on the diffusion is not available yet, and the stability of a Frank loop in copper under stress environment, simulated in this work, is not sufficient to simulate the crowdion-bundle motion at cascade process. One can expect the large diffusion length of the crowdion bundles because of the low activation energy. The process (3) above is an inverse reaction triggered by certain diffusion obstacles, for instance point defects or defect clusters invisible in microscopy. The nature of the obstacles is currently unknown. Other models may be

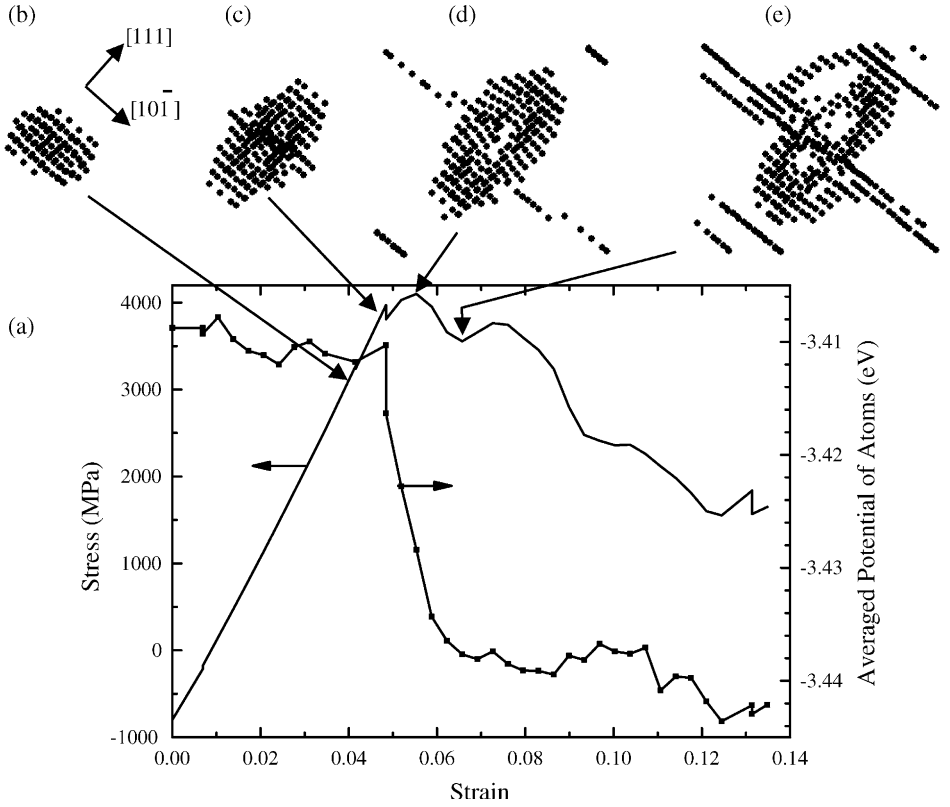

Fig. 6. MD simulation of a 19-SIA dislocation loop in copper at 0 K under compression stress. A stress–strain curve together with potential variation in (a), and behavior of a dislocation loop transforming into a crowdion bundle (b–e) are shown.

possible to describe the experimental results, such as diffusion of a dislocation loop in its habit plane and formation of another kind of mobile defect cluster. However, they were not evidenced at this moment.

4. Conclusions

Defect clusters corresponding to displacement cascades were observed by in situ TEM observations in copper under irradiations with 100 keV C^+ and 240 keV Cu^+ ions at temperatures from 573 to 823 K. The defect clusters disappeared in seconds and the lifetime depends on temperature and ion species, and on implantation fluence. We observed two or three defects appeared at the same time within the time resolution of 1/30 s under irradiation of copper ions. From their anisotropic distributions, and fluence-dependent distance ranging from 4 to 140 nm, as well as mass-dependence, we conclude that the multi-cluster formation is a single ion event, and that subcascades and mobile defect clusters formed directly from cascades are attributable to the clusters. In addition to the cascade-driven mobile defect clusters, dislocation loops also transform into the mobile ones under irradiations. The behavior is characterized as one-dimensional back-and-forth motion and spontaneous long range diffusion. Those observations suggest that the dislocation loops can transform into mobile defect clusters, diffuse along the crowdion directions, and transform again at certain diffusion obstacles which are invisible in TEM. The MD simulations on the stability of dislocation loops under compressive stress were performed and successfully detect the transformation of a loop to crowdion bundles with small potential difference and no distinct potential barrier. The results of the in situ TEM and MD in this work together with the recent MD results suggest that the mobile defect clusters are crowdion bundles.

References

[1] H. Sakaida, N. Sekimura, S. Ishino, J. Nucl. Mater. 179–181 (1991) 928.
[2] K. Fukumoto, C. Kinoshita, H. Abe, K. Shinohara, M. Kutsuwada, J. Nucl. Mater. 179–181 (1991) 935.
[3] S. Ishino, N. Sekimura, H. Sakaida, Y. Kanzaki, Mater. Sci. Forum 97–99 (1992) 165.

[4] I.M. Robertson, J.S. Vetrano, M.A. Kirk, M.L. Jenkins, Philos. Mag. A 63 (1991) 299.
[5] S. Ishino, N. Sekimura, K. Hirooka, T. Muroga, J. Nucl. Mater. 141–143 (1986) 776.
[6] S. Ishino, N. Sekimura, T. Muroga, Mater. Sci. Forum 15–18 (1987) 1105.
[7] H. Abe, C. Kinoshita, K. Nakai, J. Nucl. Mater. 179–181 (1991) 917.
[8] A. Taylor, C.W. Allen, E.A. Ryan, Nucl. Instrum. and Meth. B 24&25 (1987) 598.
[9] C. Kinoshita, H. Abe, K. Fukumoto, K. Nakai, K. Shinohara, Ultramicroscopy 39 (1991) 205.
[10] H. Abe, H. Naramoto, K. Hojou, S. Furuno, JAERI-Research 96-047.
[11] L.M. Howe, M.H. Rainville, Nucl. Instrum. and Meth. B 19&20 (1987) 61.
[12] M. Kiritani, J. Nucl. Mater. 251 (1997) 237.
[13] K. Arakawa, S. Arai, H. Orihara, K. Ono, M. Kiritani, J. Electron Microscopy 51 (2002) S225.
[14] R.E. Stoller, G.R. Odette, B.D. Wirth, J. Nucl. Mater. 251 (1997) 49.
[15] Yu.N. Osetsky, D.J. Bacon, A. Serra, B.N. Singh, S.I. Golubov, J. Nucl. Mater. 276 (2000) 65.
[16] M.A. Kirk, M.L. Jenkins, H. Fukushima, J. Nucl. Mater. 276 (2000) 50.
[17] H. Abe, S. Yamamoto, A. Miyashita, J. Electron Microsc. 51 (2002) S183.
[18] H. Abe, S. Yamamoto, A. Miyashita, K.E. Sickafus, J. Appl. Phys. 90 (2001) 3353.
[19] T. Cabioch, J.P. Riviere, J. Delafond, J. Mater. Sci. 30 (1995) 4787.
[20] A. Iwase, L.E. Rehn, P.M. Baldo, L. Funk, J. Nucl. Mater. 238 (1996) 224.
[21] H. Abe, H. Naramoto, A. Iwase, C. Kinoshita, Nucl. Instrum. and Meth. B 127–128 (1997) 681.
[22] J.F. Ziegler, J.P. Biersack, U. Littmark, The Stopping and Range of Ions in Solids, Pergamon, New York, 1985.
[23] R.S. Walker, D.A. Thompson, Radiat. Eff. 37 (1978) 113.
[24] H. Abe, Diamond Relat. Mater. 10 (2001) 1201.
[25] M.L. Jenkins, M.A. Kirk, Characterization of Radiation Damage by Transmission Electron Microscopy, Inst. of Physics Publ., 2001, p. 11.
[26] N. Yoshida, M. Kiritani, J. Phys. Soc. Jpn. 35 (1973) 1418.
[27] T. Muroga, Radiat. Eff. Def. Solids 144 (1998) 105.
[28] Y. Yang, N. Sekimura, H. Abe, Phys. Lett. A 315 (2003) 293.